IEEE Access
Multidisciplinary | Rapid Review | Open Access Journal

Received September 18, 2018, accepted October 3, 2018, date of publication October 8, 2018, date of current version October 31, 2018.

Digital Object Identifier 10.1109/ACCESS.2018.2874826

Trap Distribution and Dielectric Breakdown of Isotactic Polypropylene/Propylene Based Elastomer With Improved Flexibility for DC Cable Insulation

YU GAO [1,2], (Member, IEEE), JING LI [1], YANQIU YUAN [1], SHIHAO HUANG [1], AND BOXUE DU [1], (Senior Member, IEEE)

[1]School of Electrical and Information Engineering, Tianjin University, Tianjin 300072, China
[2]School of Electronics and Computer Science, University of Southampton, Southampton SO17 1BJ, U.K.

Corresponding author: Yu Gao (hmgaoyu@tju.edu.cn)

This work was supported in part by the National Natural Science Foundation of China under Grant 51677127 and in part by the National Basic Research Program of China (Program 973) under Grant 2014CB239501 and Grant 2014CB239506.

ABSTRACT In this paper, we report on electrical and mechanical properties of isotactic polypropylene (PP) blended with polyolefin elastomer (POE) and propylene-based elastomer (PBE). Carrier trap distribution of the samples was estimated by isothermal surface potential decay measurement, while dc breakdown strength was measured through a pair of semicircle electrodes. Elongation at break and tensile strength were obtained to examine the variation in mechanical property of PP caused by the addition of elastomers. Furthermore, scanning electron microscope (SEM), differential scanning calorimetry (DSC), and dynamic mechanical analysis (DMA) have been employed to assist the understanding of morphology of the blends, thermal properties, and mechanical properties. Obtained results have indicated that with the increase of the elastomer content from 0 to 30 wt%, the trap depth appeared to be shallower and the dc breakdown strength tended to be reduced for both PP/PBE and PP/POE samples. Compared with PP/POE blend, PP/PBE blend had deeper trap depth, which should be responsible for its higher dc breakdown strength. In addition, PP/PBE blend has presented a better performance in elongation at break and tensile strength measurement. With the growth of the elastomer content, the crystallinity of the blends appeared to decrease, whereas the melting and the crystallization temperatures did not change remarkably. The SEM inspections and DMA results revealed better compatibility between PP and PBE compared with that between PP and POE, which should be the reason for the better electrical and mechanical properties of PP/PBE blend. The blend of PBE with low content could result in remarkably improved flexibility of PP with acceptable electrical strength for dc cable insulation.

INDEX TERMS Polypropylene, propylene based elastomer, polyolefin elastomer, trap distribution, DC breakdown strength, elongation at break, tensile strength.

I. INTRODUCTION

High Voltage Direct Current (HVDC) transmission which has the advantages of low transmission loss, high stability and low cost has been widely developed as an important power delivery method in the world [1]–[3]. In recent years, the HVDC transmission through underground or submarine cables has been reported [4], [5]. In these cables, cross-linked polyethylene (XLPE) is often selected as the primary insulation material owing to its excellent electrical and mechanical properties [6]–[8]. The length of the XLPE insulated DC power cable is growing year by year. Thus the insulation property of the cable becomes a serious concern for the safe operation of the HVDC transmission system [6], [7]. With the growth of voltage level for HVDC transmission, the energy delivered through DC XLPE is expected to be higher, as a result of which the carrying capacity of the cable tends to be enhanced [8]. However, due to the relatively low melting point of XLPE as well as the limitation from electric field distortion, the maximum operating temperature of DC XLPE cable is usually limited at 70 °C [9].

In addition, the microstructure of XLPE is featured with a three-dimensional network by which thermal endurance of the material could be certainly expected [10]. However, as the XLPE insulation gets close to the end of its lifetime, its disposal appears to be difficult, thus incineration or landfill becoming the unavoidable way [11], which inevitably introduces environmental problems. Therefore, both from the viewpoints of environmental protection and carrying capacity enhancement, the development of a novel material for DC power cable insulation becomes an urgent issue.

Polypropylene (PP) has been utilized in a large variety of applications as insulating material in electrical equipment. It has high breakdown strength, low dielectric loss, high melting point and in particular the recyclable nature, which makes it a promising candidate for DC cable insulation [1]–[3], [12]–[14]. Investigations have been performed to estimate the material property of PP as the primary insulation of DC cable, and it has been confirmed that both syndiotactic polypropylene (s-PP) and isotactic polypropylene (i-PP) exhibit the potential of being such insulation [12]–[16]. Recently, i-PP drew increasingly attentions as being the DC cable insulation due to its higher breakdown strength and lower manufacture cost [12]–[14]. However, an important problem that may influence the industry application of i-PP as cable insulation is that the stiffness of virgin i-PP is much higher than that of XLPE. Hence its toughness should be modified [1]. In previous studies, many types of materials are selected as toughening agents to improve the flexibility of virgin PP. C.D. Green *et al.* [3] reported on optimization in composition of a propylene homopolymer/propylene-ethylene copolymer blend which had similar electrical and mechanical performances to those of XLPE. But the blend still held higher modulus than XLPE with a flatter temperature profile up to 120 °C–130 °C. Caramitu *et al.* [17] investigated the mechanical property of PP modified by various rubber elastomers, and it was pointed out that the compatibility of PP and elastomers was bad. Zha *et al.* [18] demonstrated the improved mechanical property of PP blended with styrene-ethylene-butylene-styrene block copolymer (SEBS) that had high melting point and excellent compatibility. However, the introduction of the elastomer resulted in the accumulation of space charge obviously. Zhou *et al.* [19] pointed out that the PP/POE blend with proper POE content could possess better toughness as compared with the virgin i-PP and exhibited higher DC breakdown strength than XLPE. However, as revealed in our previous work, due to bad compatibility between PP and POE, the POE acted as ''separated spots'' within the PP matrix, which may result in the formation of physical defects that reduced the DC breakdown strength of PP [20], [21]. Accordingly, in order to obtain excellent electrical property of PP/elastomer blend for DC cable insulation, the compatibility between PP and elastomer should be taken into account.

A new type of elastomer PBE, which has better compatibility with PP, has been proposed in this work. Electrical and mechanical properties of PP/PBE blend have been estimated and compared to those of PP/POE blend with various elastomer contents. It was found that remarkably improved mechanical property and excellent electrical property could be achieved with the addition of PBE of low content, which should be ascribed to the good compatibility between the PP matrix and the PBE.

II. EXPERIMENTAL SETUP

A. SAMPLE PREPARATION

Commercially available PBE (Vistamaxx 6202, Exxon Mobil Corporation, USA) and POE (DOW 8401, Dow Chemical Company, USA) were employed as toughening agents to prepare PP based blends. The i-PP base material (PPH-T03) was purchased from Sinopec Beihai, China. The PBE elastomer is composed of repetitive monomers of isotactic propylene (85 wt%) and randomly distributed ethylene (15 wt%). The PBE was prepared by means of proprietary metallocene catalyst method invented by Exxon Mobil Corporation [22]. The POE elastomer is a type of thermoplastic elastomer consisting of ethylene-octane copolymer, and the proportion of ethylene is 75 wt%. In this work, the content of elastomer was selected at 10 wt%, 20 wt% and 30 wt%, respectively. The base material and the elastomer were firstly cleaned with ethyl alcohol and were dried at 80 °C in a vacuum chamber. Then the mixture was placed into an internal mixer with temperature of 180 °C at speed of 30 r/min for 5 min. The obtained mixtures were hot pressed under 16 MPa at 190 °C for 5 min, by which the blend samples with dimension of 90 mm×90 mm could be obtained. The thickness of sample was 500 μm and 100 μm respectively for isothermal surface potential decay (ISPD) measurement and DC breakdown test. In order to easily index the blends with various types and contents of elastomers, the abbreviations of the samples are listed in detail in TABLE 1.

TABLE 1. Index for polymer samples investigated in this work.

Index	Elastomer Content	Elastomer Type	ε_r
PP	0 wt%	—	2.18
PB10	10 wt%	PBE	2.19
PB20	20 wt%	PBE	2.20
PB30	30 wt%	PBE	2.20
PBE	100 wt%	PBE	2.39
PO10	10 wt%	POE	2.22
PO20	20 wt%	POE	2.23
PO30	30 wt%	POE	2.25
POE	100 wt%	POE	2.28

B. SCANNING ELECTRON MICROSCOPE (SEM) OBSERVATION

In order to better understand the blending status between the PP base material and the elastomers, Scanning Electron

Microscope (SEM) measurement were performed to observe the micromorphology of samples. The samples were initially immersed in liquid nitrogen, after which they were mechanically bended, hence the cross-section of the sample was obtained. The smooth section was then coated with Aurum for SEM measurement. The SEM used in this work was FEI Nanosem430 (FEI Company, USA). Thermal electrons were accelerated under voltage of 10 kV, the energy of electron beam was 10 keV with beam spot 3, and the magnification was 10000.

C. DIFFERENTIAL SCANNING CALORIMETRY (DSC) MEASUREMENT

The DSC measurement was carried out by using a Perkin Elmer DSC7 at a heating/cooling rate of 10 °C/min between 25 °C and 200 °C in nitrogen atmosphere. The detailed measurement process was described as follows. First, the sample was heated from 25 °C to 200 °C and was held for 5 min to remove thermal history of the sample. Second, the temperature was reduced from 200 °C to 25 °C to obtain the crystallization curve. Finally, the temperature was raised again from 25 °C to 200 °C to get the melting curve. From the crystallization and melting curves, parameters including crystallization temperature T_c and melting temperature T_m were derived. The crystallinity of the sample was calculated by the equation below [14],

$$X_c = \frac{\Delta H_m}{\Delta H_{m0}} \times 100\% \tag{1}$$

where ΔH_m is the melting enthalpy of sample, ΔH_{m0} is the melting enthalpy for PP with 100% crystallinity and is selected as 209 J/g [1].

D. DYNAMIC MECHANICAL ANALYSIS (DMA) MEASUREMENT

Glass transition temperature (T_g) of the test sample was measured by Dynamic Mechanical Analysis (DMA) method (TA-Q800, TA Instrument, USA). The measurement was performed with 3-Point Bending mode at frequency of 1 Hz, amplitude of 20 μm and heating rate of 5 °C C/min. The temperature range of the test was −50 °C∼100 °C (−100 °C∼100 °C for pure PBE and POE). The storage modulus (E'), loss modulus (E'') were measured hence the $tan\delta$ could be calculated by the following equation. The T_g is determined by marking the peak value in the $tan\delta$ curve.

$$tan\delta = \frac{E''}{E'} \tag{2}$$

E. ISOTHERMAL SURFACE POTENTIAL DECAY (ISPD) MEASUREMENT

Carrier trap distribution could be derived from the ISPD measurement [23], [24]. The surface potential of the polymer sample is established through DC corona charging, and then is allowed to decay under isothermal condition, associated with the charge de-trapping behavior closely [24]–[26]. Accordingly, the trap distribution could be derived from the

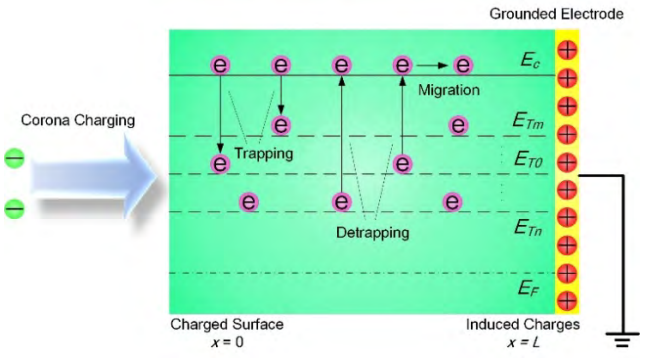

FIGURE 1. Scheme of charge trapping and de-trapping process in energy band after negative corona charging. E_c is bottom of conduction band, E_{Tn}, E_{T0} and E_{Tm} are traps of different energy levels respectively, E_F is Fermi level.

ISPD measurement. To interpret the charge transportation behavior in detail, negative charge trapping and de-trapping process in energy band is shown in Fig.1. The charged surface in Fig. 1 corresponds to the position defined as $x=0$, while the grounded electrode is regarded as the position $x = L$. Electrons could be transferred from the surface to the bulk, and then migrate towards the grounded electrode, leading to the decay of surface potential [27]. It should be mentioned that although hopping process takes place in the polymer [28], band transport is assumed as the dominate process and re-trapping event is neglected in the method [29]. Such approximations have been considered to be reasonable when film sample is analyzed [30]–[33]. The trap density has been considered closely related to the decay behavior, which could be expressed as [29], [32],

$$N(E) = \frac{\varepsilon_0 \varepsilon_r}{qkTL^2} \left| t \frac{dU_s}{dt} \right| \tag{3}$$

where $N(E)$ is the trap density occupied by carriers at trap level E, $\varepsilon_0 = 8.854187817 \times 10^{-12}$F/m is the permittivity of vacuum, ε_r is the relative permittivity of the material and is shown in TABLE 1, $q = 1.602176565 \times 10^{-19}$ C is the elementary charge, $k = 1.3806505 \times 10^{-23}$ J/K is the Boltzmann's constant, T is the Kelvin temperature in K, L is the thickness of the sample in m, t is the decay time in s, U_s is the surface potential in V. In addition, by defining the demarcation energy E_m which indicates the border between emptied and occupied traps [29], it is proposed that the E_m moves away from the band edge E_c with the lapse of time, thus the time dependent trap level $E = E_c - E_m$ can be expressed as a function of the decay time [29], [32], [33],

$$\Delta E = kT \ln(\nu t) \tag{4}$$

where ν is the attempt to escape frequency and was selected as 10^{12} s^{-1} in this work. Accordingly, the relationship between $N(E)$ and ΔE presents the trap distribution within corona charged material. As the transportation of positive charges has similar process, its diagram is not shown for space saving.

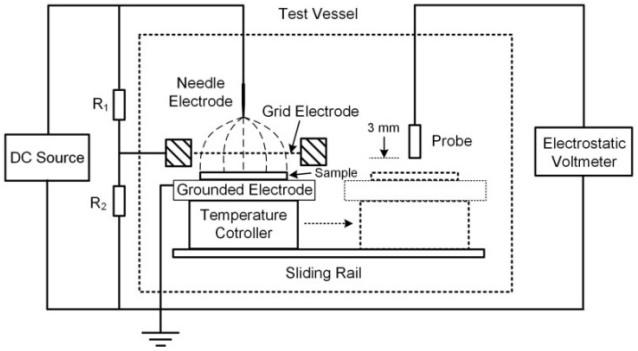

FIGURE 2. Test Circuit for ISPD measurement.

The schematic diagram of test circuit for ISPD measurement is depicted in Fig.2. The needle to plane electrode system was employed to induce corona discharge, and the grid electrode was used to control the surface potential. The needle electrode was 1 mm in diameter with a tip radius of curvature of 13 μm. The interval between the needle electrode and the sample surface was 8 mm, while the grid electrode was placed 5 mm above the surface. The potential at the needle electrode was $\pm$7 kV, the potential at the grid electrode was $\pm$3.2 kV, charging for 20 min. The temperature of the sample was kept at 40 °C so as to accelerate the potential decay, the relative humidity was controlled lower than 25%. Surface potential of the charged sample was recorded by a Kelvin type electrostatic voltmeter (P0865, Trek Co ltd., USA), the probe was positioned 3 mm above the center of sample surface. Five specimens were measured for checking the repeatability, and the typical test results were presented in this paper.

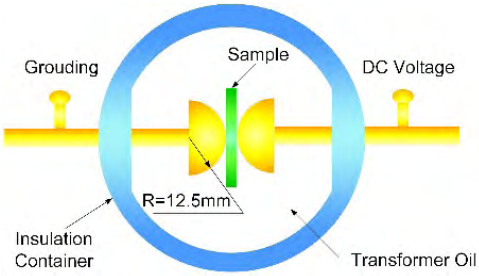

FIGURE 3. Electrode structure for DC breakdown strength test.

F. DC BREAKDOWN STRENGTH MEASUREMENT

DC breakdown strength of the blend samples was measured by using a pair of semicircle electrodes, as can be seen in Fig.3, the radius of each electrode was 12.5 mm. The blend sample of 100 μm was sandwiched by the electrodes, by which a quasi-uniform electric field could be formed across the film sample. In order to prevent surface flashover, the electrodes as well as the sample was immersed into transformer oil. DC voltage was supplied by a DC power source with maximum value of 140 kV (HTC 10 kVA/100 kV, Wuhan Sanxin Huatai Electrical Testing Equipment Co., Ltd., China). One side of the electrodes was connected to the DC source, while the other side was grounded. The DC breakdown test was performed at room temperature. The DC voltage applied was increased at a rate of 0.5 kV/s until insulation breakdown occurred in the sample. The breakdown strength was recorded as the average value of ten samples.

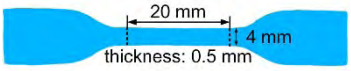

FIGURE 4. Dumbbell shaped specimen.

G. MECHANICAL PROPERTY MEASUREMENT

Mechanical properties of the test samples were measured by means of a mechanical tester (Jiangdu Jingyi Testing Machinery Co. Ltd., China) at a crosshead speed of 250 mm/min at room temperature according to ASTM D882-2010 [34]. The applied force is a variable force, which can make the crosshead speed constant. Dumbbell shaped specimen was prepared for the test, as is illustrated in Fig.4. Elongation at break and tensile strength which were considered as important parameters relating to the flexibility of the material were measured [1], [19]. At least five specimens were employed for checking the repeatability, the average values are presented in this paper.

III. RESULTS AND DISCUSSION

A. TRAP DISTRIBUTION

The typical surface potential decay behavior is depicted in Fig.5, both the cases for positive and negative corona charging are presented. It can be observed that the potential decay exhibits non-linear manner where a fast decay occurs at the initial stage that is then followed by a slow decay. Since the electric field generated by the implanted charges is as low as 5 kV/mm ~7 kV/mm, injection of charge with the opposite sign from the grounded electrode should be negligible, and carrier recombination is not taken into consideration in this paper. With the increase of elastomer content, the decay rate tends to increase for both the positive and the negative potentials. It has been demonstrated that the decay is associated with charge trapping and de-trapping processes [35]. Electric charges generated during the corona discharge process are driven by the field and migrate to the sample surface. As they arrive at the test specimen, charge transfer is considered to occur and the charge within the sample bulk becomes electronic in nature [31], [36]. Due to the presence of carrier traps as stated earlier in this paper, the charges could be captured firstly and are then thermally activated to de-trap and transport to the grounded electrode, leading to the decrease of surface potential [27]. It has been suggested by G. Chen et al that both deep and shallow traps are likely to contribute to the de-trapping process [35]. The initial fast decay of the potential should be ascribed to charge de-trapping from shallow traps, while the following slower decay of the potential is due to charge de-trapping from deep traps. As can be found in Fig.5(a) and Fig.5(b), the test data are in good

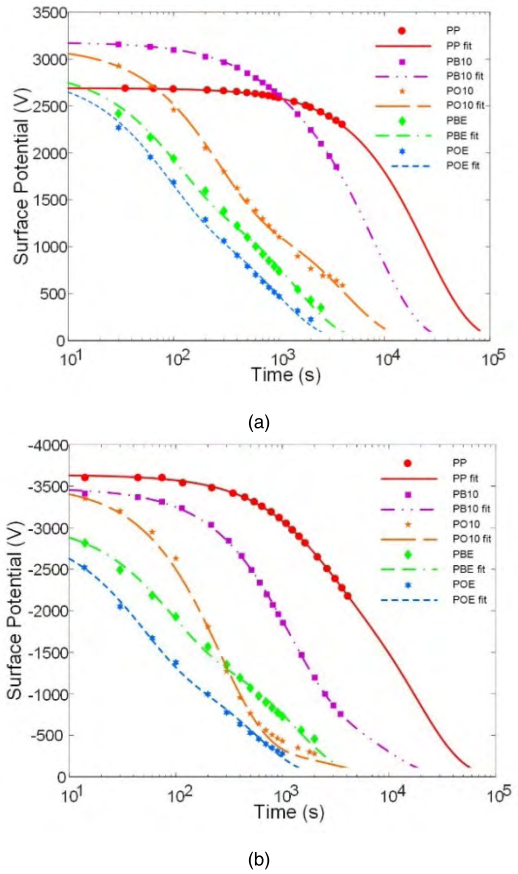

FIGURE 5. Typical surface potential decay behavior. (a) Positive charge. (b) Negative charge.

agreement with the fitting curve as bi-exponential function. The motivation that a bi-exponential function is employed to fit the test data is not only based on our experience but on the basis of physical origin. It has been claimed that the thermal de-trapping probability of trapped charge P_{de} can be expressed by [31],

$$P_{de} = \nu \exp(-\frac{\Delta E}{kT}) \tag{5}$$

Accordingly, by assuming that the dissipation of trapped charge is induced by the de-trapping from both shallow and deep traps, the density of trapped charge can be expressed by [37],

$$N(t) = N_s \exp(-k_s t) + N_d \exp(-k_d t) \tag{6}$$

where $N(t)$ is the density of total trapped charge, N_s is the density of charge captured by shallow trap, N_d is the density of charge captured by deep trap, k_s and k_d are de-trapping rate for shallow and deep traps, respectively. Since the decay of surface potential is closely related to the release of charge from both shallow and deep traps, the variation in surface potential with time is proposed as [31],

$$U_s = A \exp(\alpha t) + B \exp(\beta t) \tag{7}$$

where A, B are fitting parameters related to the potentials excited respectively with charges captured by shallow and deep traps, α, β are the parameters with respect to the de-trapping rates of charges captured by shallow and deep traps. In our research, the bi-exponential function (7) is used to describe the decay behavior of surface potential. Taking the negatively charged PP as an example, the fitting parameters are A=1088 V; B=2549 V;α=-4.89×$10^{-4}s^{-1}$; β=-5.46×$10^{-5}s^{-1}$; And the R-squared R^2=0.9999. Therefore, the fitting curves are employed for trap distribution calculation in the following section.

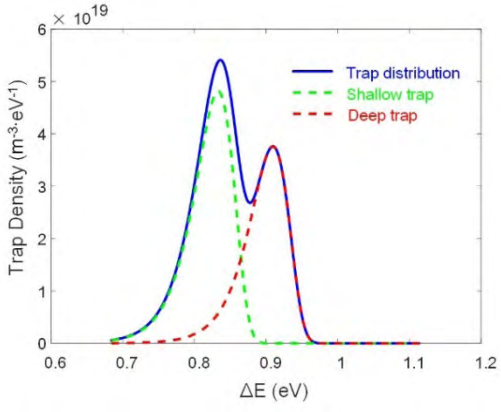

FIGURE 6. Typical distribution of carrier trap derived from ISPD measurement.

The typical trap distribution feature is shown in Fig.6 by taking hole trap of PO10 as an example. The trap depth covers a certain range from 0.68 eV to 0.97 eV, and two peaks are formed respectively at 0.83 eV and 0.91 eV, which are referred to as shallow and deep trap centers. In order to better describe the feature of shallow or deep trap, the two peaks are separated so as to illustrate the individual shallow and deep trap distributions, as is shown in Fig.6 by the green and the red dash lines.

Since both positive and negative corona charging have been performed, the trap distributions for hole and electron in the blends with various elastomer contents could be examined. The typical deep and shallow trap distributions for holes in the samples are shown in Fig.7 and Fig.8, respectively. The deep trap distribution of hole in PP/PBE blend is shown in Fig.7(a). With the increase of the elastomer content, the trap distribution curve appears to move left. For instance, the deep trap for hole in virgin PP covers the range from 0.8 eV to 1.01 eV and has the trap center at 0.958 eV. As regards the sample PB30 which contains 30 wt% of PBE elastomer, the trap distribution covers the range from 0.72 eV to 0.92 eV and the trap center is at 0.884 eV. In particular, the deep trap distribution of hole in virgin PBE is also depicted as a comparison, and it is between 0.71 eV and 0.92 eV with a peak at 0.88 eV. This strongly suggests that the addition of PBE elastomer decreases the energy level of deep trap. Furthermore, it is also noticed that the trap density appears

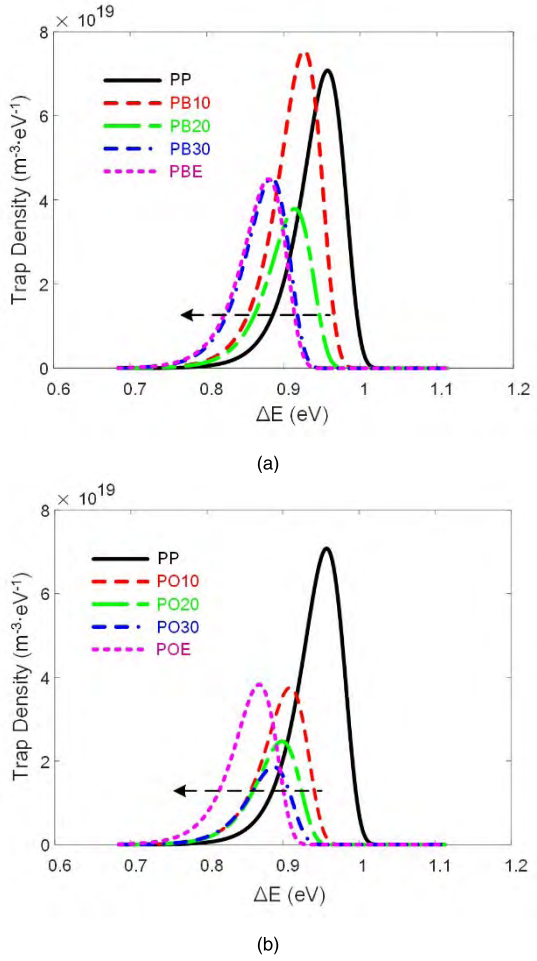

FIGURE 7. Deep trap distribution for hole for the two types of blends. (a) PP/PBE blend. (b) PP/POE blend.

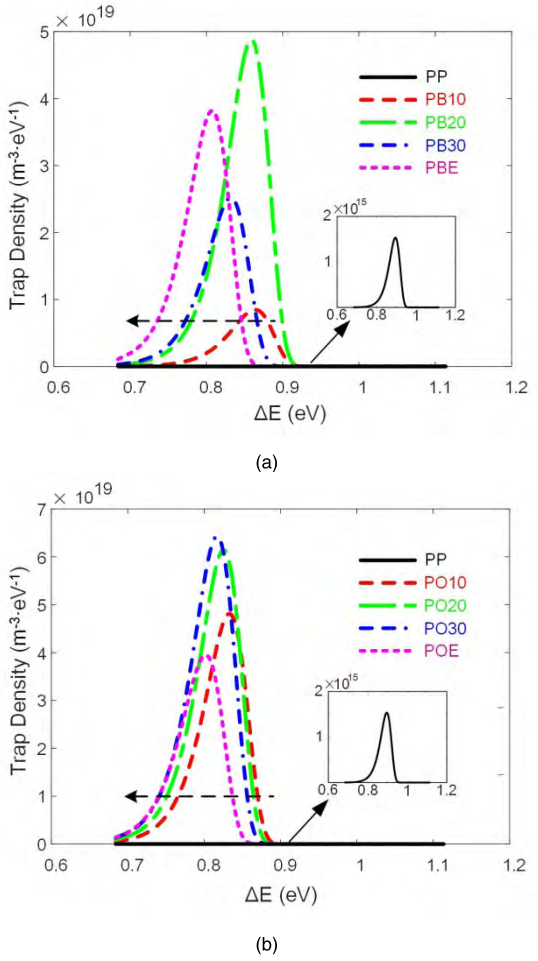

FIGURE 8. Shallow trap distribution for hole for the two types of blends. (a) PP/PBE blend. (b) PP/POE blend.

to reduce as the content of PBE elastomer grows from 0 wt% to 30 wt%. Similar behaviors are observed for the PP/POE blend as shown in Fig.7(b). The deep trap becomes shallower with the growth of POE content, and the trap density also remarkably decreases. By comparing the curves presented in both Fig.7(a) and Fig.7(b), it is found that the reduction in trap depth and trap density for PP/POE blend are more considerable than that for PP/PBE blend.

The shallow trap distributions for hole in both PP/PBE and PP/POE blends are shown in Fig.8. As can be observed in Fig.8(a), an obvious reduction in shallow trap center occurs as PBE is added into the virgin PP. The shallow trap center is at 0.895 eV for virgin PP, whereas such trap center moves left to 0.864 eV for PB10. It means that the presence of PBE could result in decrease in the shallow trap center. With the increase of the PBE content from 10 wt% to 30 wt%, the trap center reduces to 0.832 eV which is close to the value of virgin PBE at 0.808 eV. Furthermore, it is also noticed that the density of shallow trap of the blend is higher than that of virgin PP. For instance, the density at trap center for virgin PP is only 1.5×10^{15} $m^{-3}\cdot eV^{-1}$, but suddenly this value rises to the order of 10^{19} $m^{-3}\cdot eV^{-1}$ with the presence of PBE elastomer. As regards the PP/POE blend, similar behavior in the variation of trap depth and trap density is found in Fig.8(b). However, as compared with the PP/PBE blend, the addition of POE leads to more remarkable decrease in trap depth. In addition, the shallow trap density exhibits a significant growth as the content of POE increases, which indicates again that more shallow traps are introduced in the blend sample.

Deep trap distributions for electron for both PP/PBE and PP/POE blends with various elastomer contents are shown in Fig.9(a) and Fig.9(b). As regards the PP/PBE blend, as shown in Fig.9(a), with the increase of the PBE content, the trap distribution curve shifts towards left. It can be seen that the virgin PP covers the deep trap range from ∼0.76 eV to ∼1.00 eV, while the PB30 exhibits a trap distribution range from ∼0.73 eV to ∼0.94 eV, which is remarkably lower than that for the virgin PP. As a comparison, the deep trap distribution for virgin PBE is also presented, the trap distribution starts from 0.71 eV to 0.94 eV. Furthermore, as the PBE is added, the density at trap center tends to reduce. It can be found that the density at trap center for PB10, PB20 and PB30 is in the range from 2.23×10^{19} $m^{-3}\cdot eV^{-1}$

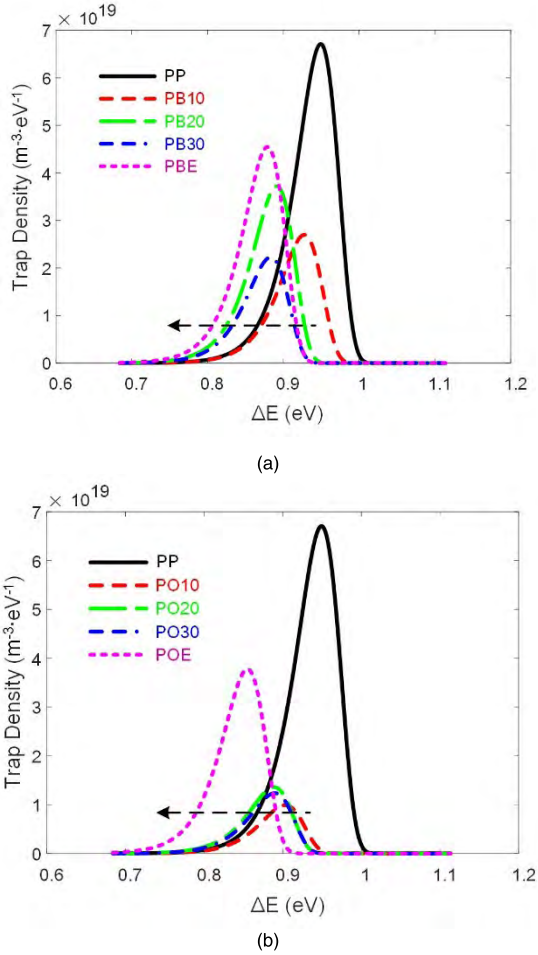

FIGURE 9. Deep trap distribution for electron for the two types of blends. (a) PP/PBE blend. (b) PP/POE blend.

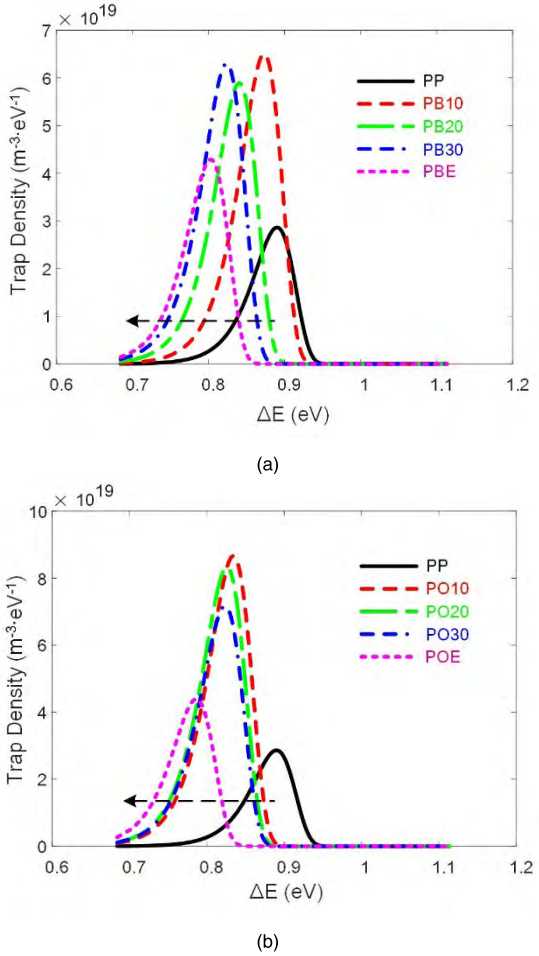

FIGURE 10. Shallow trap distribution for electron for the two types of blends. (a) PP/PBE blend. (b) PP/POE blend.

to 3.72×10^{19} $m^{-3}\cdot eV^{-1}$, which is only one third to half the value of the virgin PP ($6.71\times10^{19}m^{-3}\cdot eV^{-1}$). As for the PP/POE blend, the trap depth appears to be shallower with the growth of elastomer content as well. Another important fact is that the density at trap center for the PP/POE blend become reduced as compared with the virgin PP by a factor of ∼6, which is more significant than that in the PP/PBE blend. The variation of POE content from 10 wt% to 30 wt% doesn't induce obvious change in the density at trap center, which are close to 1.0×10^{19} $m^{-3}\cdot eV^{-1}$. It is then concluded from Fig.9(a) and Fig.9(b) that the presence of elastomers leads to the reduction in both trap depth and trap density for electron in the virgin PP, and such a reduction is more obvious in PP/POE than in PP/PBE blend.

Fig.10 shows the distributions of shallow electron trap for both PP/PBE and PP/POE blends with various elastomer contents. The distribution of shallow electron trap for PP/PBE blend is shown in Fig.10(a). With the increase of the elastomer content, the trap depth tends to be shallower obviously. The trap center is reduced from 0.889 eV for virgin PP to 0.824 eV for PB30. The virgin PBE has even shallower trap center at 0.803 eV. As for the density at trap center, it is noticed that an enhancement of the density occurs with the addition of PBE elastomer by a factor of ∼2 than the virgin PP. The trap distribution for PP/POE blend is illustrated in Fig.10(b). The presence of POE elastomer leads to the shallower of electron trap as well. On the other hand, the density at trap center becomes increased with the presence of POE elastomer. The PP/POE blend has the density at trap center in the range of $7\times10^{19}m^{-3}\cdot eV^{-1}$ ∼$9\times10^{19}m^{-3}\cdot eV^{-1}$, which is higher than that for the virgin PP (2.86×10^{19} $m^{-3}\cdot eV^{-1}$) by a factor of 2-3. By comparing the electron trap distribution curves presented in Fig.10(a) and Fig.10(b), it is assumed that the addition of POE leads to more remarkable increase in the density of shallow trap than that of PBE.

It must be argued that due to the randomness of corona discharge [31], the imperfections of polymer samples which are originated from the semi-crystal morphology of PP and the non-ideally uniform dispersion of elastomer, it is almost impossible to allow the samples to be charged under completely identical conditions. The deviations in test data caused by the inhomogeneity in polymer sample and the discharge randomness are therefore un-avoidable. The influence of the elastomer content on the trap center for hole and electron

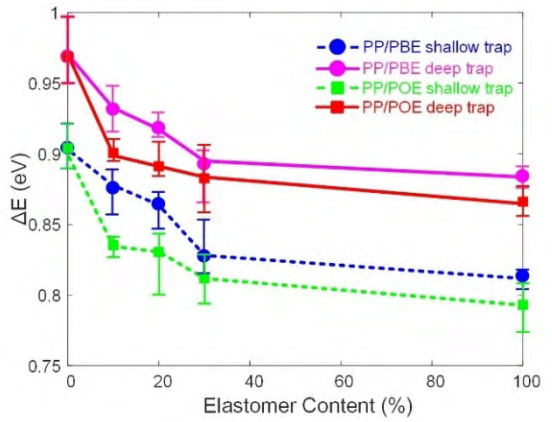

(a)

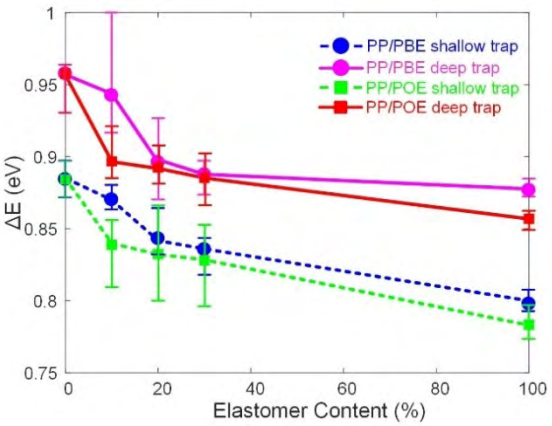

(b)

FIGURE 11. Relationship between the trap center and the elastomer content for hole and electron for the PP/elastomer blends. (a) Hole trap. (b) Electron trap

TABLE 2. Density at hole trap centers.

Samples	Trap Density ($\times 10^{19}$m^{-3}·eV^{-1})		Typical $k_{d/s}$
	Deep trap	Shallow trap	
PP	6.19~7.08	0.00015~0.00051	47200
PB10	7.12~7.55	0.75~0.85	8.882
PB20	3.64~3.88	4.57~4.91	0.777
PB30	3.55~5.47	2.02~3.33	1.798
PBE	4.39~4.66	2.96~3.82	1.178
PO10	2.59~4.95	4.32~5.60	0.782
PO20	1.84~2.47	6.14~6.52	0.402
PO30	0.96~2.34	5.43~6.75	0.289
POE	3.31~3.83	3.73~5.01	0.970

TABLE 3. Density at electron trap centers.

Samples	Trap Density ($\times 10^{19}$m^{-3}·eV^{-1})		Typical $k_{d/s}$
	Deep trap	Shallow trap	
PP	6.09~6.71	2.86~3.26	2.346
PB10	1.62~2.70	6.04~6.50	0.415
PB20	3.02~3.94	4.69~5.89	0.632
PB30	1.98~3.55	5.88~6.39	0.354
PBE	3.67~4.55	2.96~4.29	1.061
PO10	0.87~1.32	7.98~8.66	0.114
PO20	1.05~1.36	8.03~8.49	0.163
PO30	0.78~1.24	7.17~8.60	0.173
POE	3.78~5.27	2.73~4.39	0.861

is summarized in Fig.11. The average value of trap depths derived from the five measurements and the deviations are presented. As the content grows from 0 wt% (virgin PP) to 100 wt% (virgin PBE or POE), the trap center exhibits a clear decreasing tendency. It is noticed that the trap center of PP/PBE is basically higher than that of PP/POE for both shallow and deep traps. Moreover, there is no pronounced difference between the electron trap center and the hole trap center, as depicted in Fig.11(a) and Fig.11(b). The trap density at the center is summarized in TABLE 2 and 3. It can be found that as the elastomer, either PBE or POE, is blended into the PP base matrix, the deep trap density becomes reduced whereas the shallow trap density gets increased for both electron and hole. The $k_{d/s}$ that refers to the ratio of deep trap density to shallow trap density at the center is calculated to estimate the behavior of carrier trap in response to the variation in elastomer content. It is clear that the $k_{d/s}$ for PP/PBE or PP/POE blend is significantly decreased as compared with the virgin PP, which indicates that with the addition of the elastomer, shallow trap would play a more important role in determining the transportation behavior of charge carriers. It is also noticed that the virgin POE and the virgin PBE hold lower $k_{d/s}$ than that of virgin PP, which is considered as one candidate reason for the relatively low $k_{d/s}$ in the blends. Another interesting feature that could be derived from TABLE 2 and 3 is that for both electron and hole traps the virgin PBE possesses higher $k_{d/s}$ than the virgin POE, and the PP/PBE blend exhibits higher $k_{d/s}$ than the PP/POE blend. This reveals that the introduction of PBE into the PP matrix would be more beneficial from deep trap than that of POE. In addition, the total integrated trap density is not calculated and compared. Since the trap center plays a dominant role in determining the charge transportation behavior in polymer, attentions are usually paid to the energy level and density at trap center [31], [38]. Thus, the effect of elastomer on trap characteristics at the center is mainly discussed in this paper.

Assuming that the observed surface potential decay is predominantly due to charge transport through the material bulk, it is possible to estimate the bulk conductivity of materials by the following equation [30], [36],

$$\sigma = \left| \frac{\varepsilon}{U_s} \frac{dU_s}{dt} \right| \tag{8}$$

where σ is the bulk conductivity of the material, $\varepsilon = \varepsilon_0\varepsilon_r$ is the permittivity of the material. The derived values can then be tested for agreement with different models of field dependent conductivity, such as Poole-Frenkel model (PF) [30], [36],

$$\sigma(U_s) = \sigma_0 \exp(\beta_{PF} U_s^{0.5}) \tag{9}$$

where β_{PF} is the Poole-Frenkel effect coefficient, which is defined as

$$\beta_{PF} = \frac{q}{kT}\sqrt{\frac{q}{\pi\varepsilon L}} \tag{10}$$

where $\pi = 3.141592654$ is the ratio of circumference to diameter. The relationship between the bulk conductivity and the square root of the surface potential (U_s) is shown in Fig. 12. The results for PP, PB20 and PO20 charged with negative corona are depicted as examples. To better display the relationship between $lg(\sigma)$ and $U_s^{0.5}$, the logarithmic coordinate is used in longitudinal axis. With the decrease of U_s, the $log(\sigma)$ gradually decreases and tends to be a stable value of σ_0, which is in the range of 10^{-15} S·m^{-1} ~10^{-14} S·m^{-1}. The β_{PF} is then estimated according to the slope and is marked in Fig. 12. On the basis of equation (10), the ε_r can be calculated in turn as 2.47, 2.62 and 2.11 for PP, PB20 and PO20, respectively. Such values are close to the measured ones, and it is suggested that charge transportation through Poole-Frenkel mechanism possibly occurs within the sample bulk.

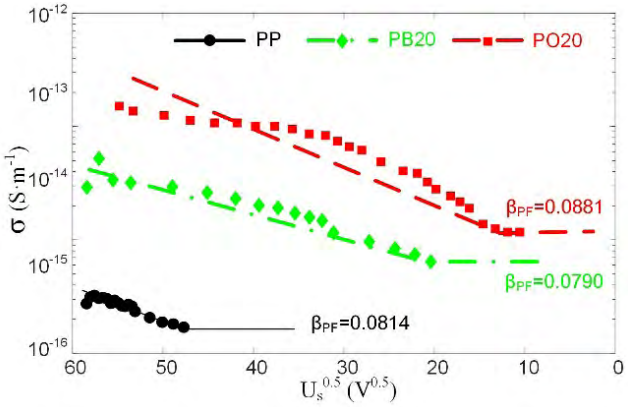

FIGURE 12. Relationship between the bulk conductivity and the square root of surface potential.

B. DC BREAKDOWN STRENGTH

DC breakdown strength is an important parameter to estimate the insulation performance of polymers. It has been pointed out that the interfacial region between the polymer base material and the fillers usually plays a key role in dielectric breakdown behavior [39], and deep traps have remarkable influence on the short-term breakdown behavior [40]. As mentioned in the above section, the density of deep trap decreases by the introduction of elastomers, while on the other hand the density of shallow trap increases.

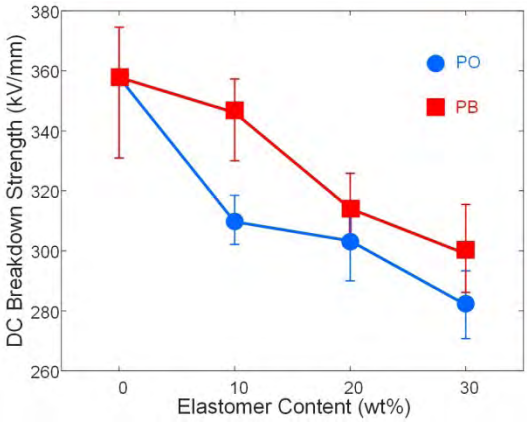

FIGURE 13. Dependence of the DC breakdown strength upon the elastomer content for both PP/PBE and PP/POE blends.

The estimation of DC breakdown strength of the blends is expected to be carried out to reveal the influence of trap on the insulation performance. Fig.13 shows the relationship between the DC breakdown strength and the elastomer content for both PP/PBE and PP/POE blends. It can be observed that the breakdown strength of virgin PP is ~358 kV/mm, which is higher than that of XLPE (~320 kV/mm) [40]. As the elastomers are blended in the virgin PP, the breakdown strength is obviously reduced, and with the increase of the elastomer content, the DC breakdown strength tends to decrease monotonically. As the elastomer content reaches 30 wt%, the breakdown strengths of PP/PBE and PP/POE are respectively ~300 kV/mm and ~280 kV/mm, obviously lower than that of XLPE. It indicates that the addition of elastomer results in unacceptable DC breakdown strength for cable insulation if the elastomer content is too high. It is also noticed that the breakdown strength of PP/PBE is higher than that of PP/POE. In particular, the breakdown strength of PB10 is ~348 kV/mm, which is over that of XLPE. This suggests that the addition of PBE elastomer with low content (10 wt%) could meet the basic requirement in electrical performance for DC cable insulation.

C. MECHANICAL PROPERTY

In order to estimate the effect of elastomers on mechanical properties of blends, elongation at break and tensile strength of the samples have been measured. Such two parameters are selected to show the toughness modification performance, which have been widely employed in previous works [1], [13], [19], [41]–[43]. It should be mentioned that a thorough examination on mechanical property is certainly needed for industry application of PP/elastomer blends, however, since the very issue discussed in this paper is the electrical property, other mechanical properties are not taken into consideration and further work in this respect will be performed in the future.

The relationship between the elongation at break and the elastomer content for both PP/PBE and PP/POE blends is

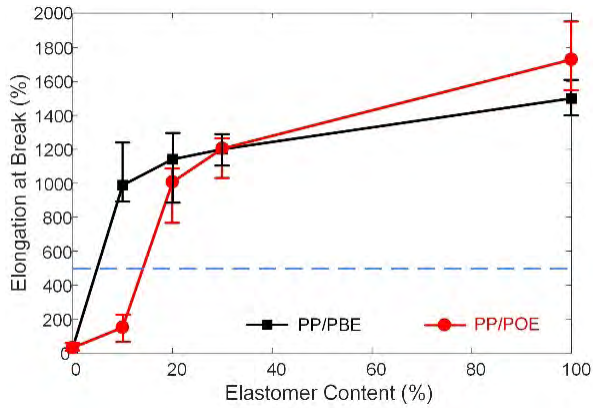

FIGURE 14. Relationship between the elongation at break and the elastomer content.

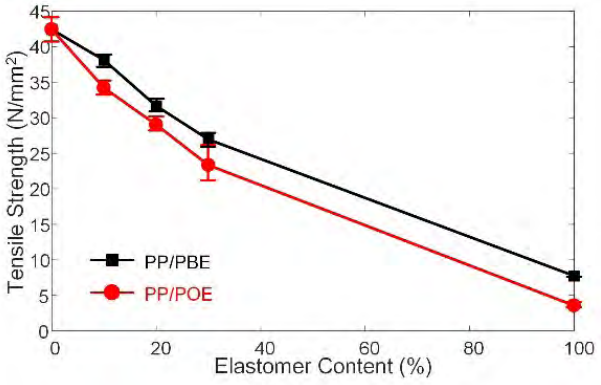

FIGURE 15. Relationship between the tensile strength and the elastomer content.

illustrated in Fig.14. With the growth of the elastomer content from 0 wt% to 30 wt%, the elongation at break increases elastomer content for both PP/PBE and PP/POE blends significantly from ∼ 40% to ∼ 1200%. It reveals that the flexibility of virgin PP is remarkably improved. The addition of PBE possesses better performance in flexibility modification than that of POE, especially at low elastomer content. However, the elongation at break of POE is higher than that of PBE. That may be due to that PP and PBE have similar structures and the compatibility of them is better. PP and PBE molecules bond closely, so the toughening effect is more significant. It can be observed that the addition of PBE with 10 wt% contributes to the elongation at break of ∼988.5%, which is higher than that of XLPE insulation (∼500%) [44]. This suggests that the addition of PBE elastomer with low content could lead to remarkable improvement on the flexibility of virgin PP. Fig.15 shows the influence of elastomer content on tensile strength of PP/PBE and PP/POE samples. The tensile strength decreases obviously as the elastomer content increases from 0 wt% to 30 wt%, and that of pure elastomers is the lowest. PP/PBE has higher tensile strength than PP/POE, which indicates that the PP/PBE has better mechanical property than PP/POE. It is also found that the tensile strengths for both PP/PBE and PP/POE are higher than XLPE (∼ 25 N/mm^2) [43] with the elastomer content no higher than 20 wt%. By considering the content dependence of elongation at break and tensile strength, it is proposed that acceptable mechanical property for recyclable cable insulation could be achieved by the addition of PBE elastomer with low content.

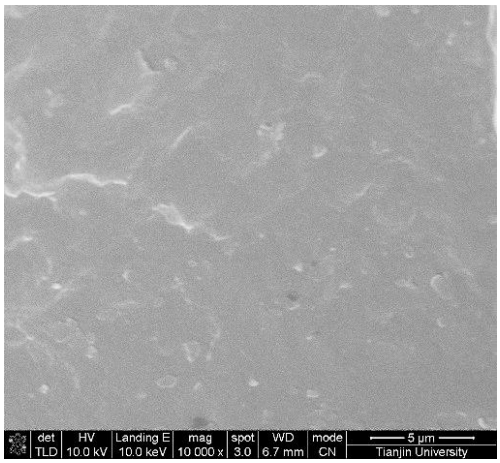

FIGURE 16. SEM photo at cross-section for virgin PP.

D. SEM ANALYSIS

With the purpose of better understanding the variation in electrical and mechanical properties caused by the addition of PBE and POE elastomers, the microstructure of the PP based blends has been inspected through SEM. The microstructures of virgin PP and the elastomer dispersion manners in PP are illustrated by SEM images respectively in Fig.16 and Fig.17. It can be seen in Fig.16 that the microstructure of virgin PP presents a mono-phase manner, where the cross-section is smooth and no obvious segments could be observed. With regard to the PP/PBE and the PP/POE blends, the morphology at the cross-section shows rather different features from the virgin PP. In PP/POE blend, the POE distributes in a disperse way within the base material. A number of isolated spots exist in the PP, and with the increase of the POE content, the size of isolated spot appears to be larger, as can be found in Fig.17(a)-Fig.17(c). This may reveal that the PP and the POE have bad compatibility, which should be attributed to the fact that the two materials have different chemical groups [19]. It has been generally accepted that the Van der Waals' force between organics with same or similar groups is higher than that with different groups [45], so the compatibility would be better for the polymer matrix and the elastomer with same or similar groups. In this work, the Van der Waals' force between POE molecular chains would be expected to be higher than that between PP and POE molecular chains. Accordingly, as can be seen in Fig.17(a) to Fig.17(c), the POE elastomers are gathered and act as ''separated spots'' within the base PP matrix due to the separation of molecular chains microscopically. As the content of POE increases, the size of the ''separated spots'' appears to grow, which implies

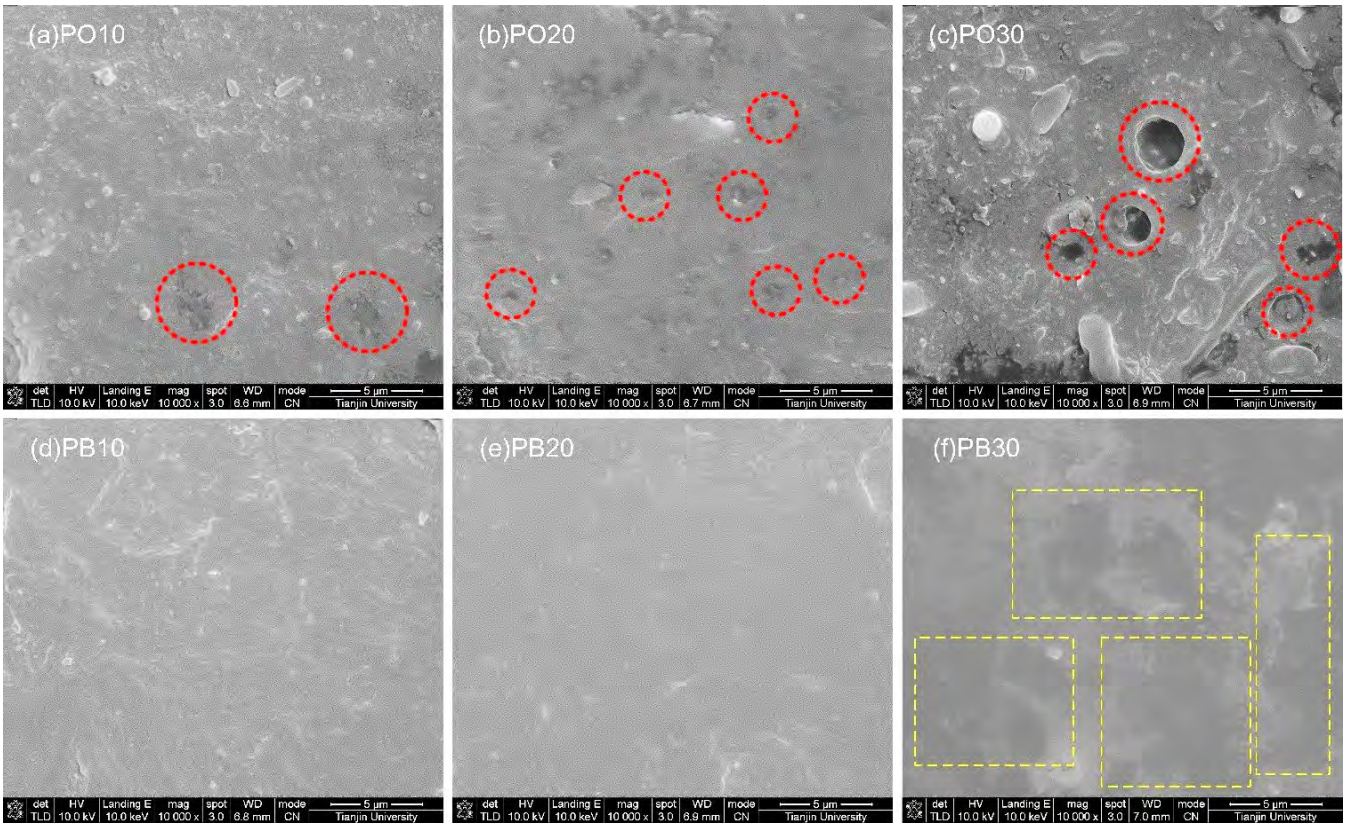

FIGURE 17. SEM photos for the PP/POE and the PP/PBE blends with various elastomer contents.

the enhancement in incompatibility between the base material and the elastomer. It could be expected that the introduction of POE into PP leads to the formation of physical defects at the interface between PP and POE due to the bad compatibility.

However, no such ''separated spots'' could be found in PP/PBE blend, as shown in Fig.17(d) to Fig.17(f). The micromorphology of the cross-section for PB10 and PB20 are rather smooth without visible distinct boundaries between the PP and the PBE, which reveals the excellent compatibility between the matrix and the elastomer. As for the PB30, the boundaries between the PP and the PBE are obvious, which are more likely as the features of ''coastline'', as indicated by the yellow dash line in Fig.17(f). As compared with the PO30, the PB30 still presents better blending performance where no abrupt interfaces between the two materials are likely to be observed. The fact that PBE possesses better compatibility with PP could be ascribed to its nature in chemical composition. The PBE elastomer is a type of mixture that contains isotactic propylene and ethylene. The Van der Waals' force between PP chains and isotactic propylene molecules of PBE is considered to be stronger. Thus PP/PBE blend exhibits better compatibility as compared with PP/POE. In addition, the ethylene groups of PBE have weak interaction with the base PP matrix, and they are more easily to be combined together. On the basis of SEM photos shown

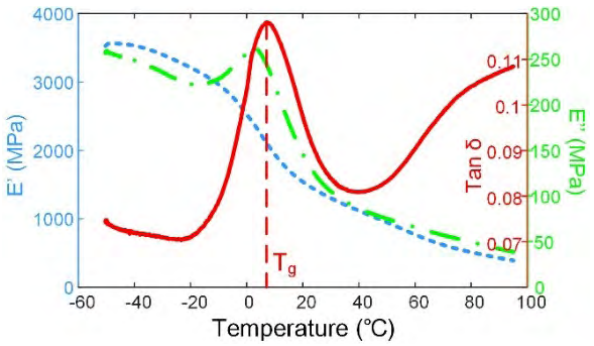

FIGURE 18. DMA curves for virgin PP.

in Fig.17, it is assumed that combination between the isotactic propylene components of PBE and the PP matrix are tight due to the higher content of the isotactic propylene in PBE (85 wt%). Thus the boundaries between PP and PBE could not be observed at low content of the elastomer. As the PBE of 30 wt% is blended into PP, the boundary profile could be clearly seen since the gathering of ethylene monomers is considerable. It has to be mentioned that due to the interaction between the PP base material and the isotactic propylene component of the PBE elastomer, the boundaries between them are much smoother than that between the PP and the POE, as shown in Fig.17(c) and Fig.17(f).

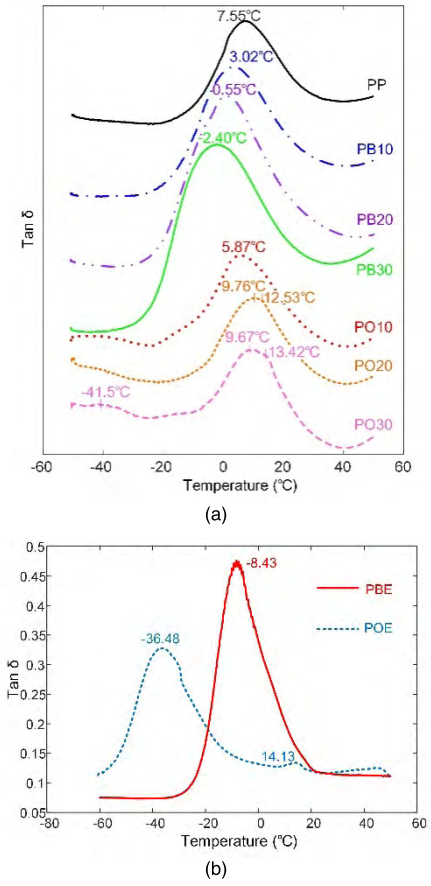

FIGURE 19. Relationship between the tanδ and the temperature for PP, elastomers and their blends. (a) tanδ curves for PP and its blend samples. (b) tanδ curves for pure elastomers samples.

E. DMA MEASUREMENT

The results of DMA measurement for virgin PP are shown in Fig.18. A decreasing trend in the storage modulus (E') over the whole temperature range is observed. When the temperature is lower than the glass transition temperature (T_g), PP is in glassy state and its E' is high. When the temperature is higher than T_g, PP is in high-elastic state and its E' decreases rapidly. In addition, the loss modulus (E'') increases first and then decreases with the increase of temperature, as shown in Fig. 18 by the green line. The ratio of E'' to E' is measured as the mechanical loss or the damping factor ($tan\delta$), which represents the elasticity of the material. When the viscoelastic material is subjected to alternating stress, the loss angle δ is the phase angle that the strain phase lags behind the stress phase. The temperature at which the peak of $tan\delta$ appears can be used to characterize the transition between the glassy state and the high-elastic state, which is referred to as the glass transition, and the temperature is T_g. The curves for $tan\delta$ of PP and PP/elastomer blends over the range from -50 °C to 50 °C are depicted in Fig.19(a). A single peak can be found for virgin PP at 7.55 °C, which is in agreement with the previous study [46]. As for PP/PBE blends, the single peak is observed as well, and the T_g tends to decrease with the increase of PBE. As regards the PP/POE blends, a single peak appears in the $tan\delta$ curve for PO10, but the double-peak feature gradually occurs with the POE content increases further to 20 wt%, and another peak appears in PO30. The separation of peaks indicates that the compatibility of PP and POE becomes worse with the increasing of POE content. For further discussion of the compatibility between PP and elastomers, the curves of pure PBE and POE are shown in Fig.19(b). It is obvious that the T_g of PBE is -8.43 °C and is close to the T_g of PP, revealing a good compatibility of PP and PBE. However, two peaks can be observed in $tan\delta$ curve for POE at -36.48 °C and 14.13 °C. Accordingly, the peak at -41.5 °C in PO30 should be introduced by POE, whilst the small peak near 10 °C is due to the peak at 14.13 °C for pure POE. Such separated-peak feature of PP/POE blends certainly indicates the bad compatibility of them. Such a result is in good agreement with the SEM inspections depicted in Fig.17.

Carrier traps in polymer insulating materials which are known as localized states presented at forbidden band are considered to be originated from chemical and/or physical defects within the polymer matrix [25], [26]. One particular type of defects that plays an important role in determining trap feature is interface. The interface in polymer is usually referred to the boundary between two parts with different properties, e.g. the interface between crystalline and amorphous regions in a semi-crystalline polymer like polyethylene [47]. Due to the disappearance of continuity in molecular chain arrangement, some chemical and/or physical disorder in chain alignment would be presented at the interface, by which the carrier traps are formed. It has been revealed that the fold of molecular chain, chain branch and cavity or void could be found at the interface between crystalline and amorphous regions in XLPE [48]. The carrier trap formed at the interface could be understood from the viewpoint of energy structure as well. It has been reported by previous studies that when charge carriers transfer across the interface, the energy band bending and drifting occur because of the difference in Fermi levels at the different materials, which results in an extra potential barrier at the interface. Such a potential barrier could lead to charge trapping at the interface [49]. In short, the presence of interface contributes to the formation of carrier traps, which would allow charge trapping and de-trapping dynamics, thereby influencing the electrical performance of polymer insulation.

In this research, interfaces appear between the PP matrix and the elastomers as shown in Fig.17, and their influence on trap characteristics should not be neglected. In order to better elucidate the possible mechanism of such interfaces in varying the trap characteristics, a schematic diagram is presented in Fig.20. It is considered that the carrier traps within PP blend should be originated from three routes, i.e. PP matrix, elastomer and interface between them. Since both the PBE and the POE elastomers have shallower traps as compared with the virgin PP, it is reasonable that the blending of elastomer results in shallower trap in the PP/elastomer blend. Furthermore, since the PBE and the POE have different

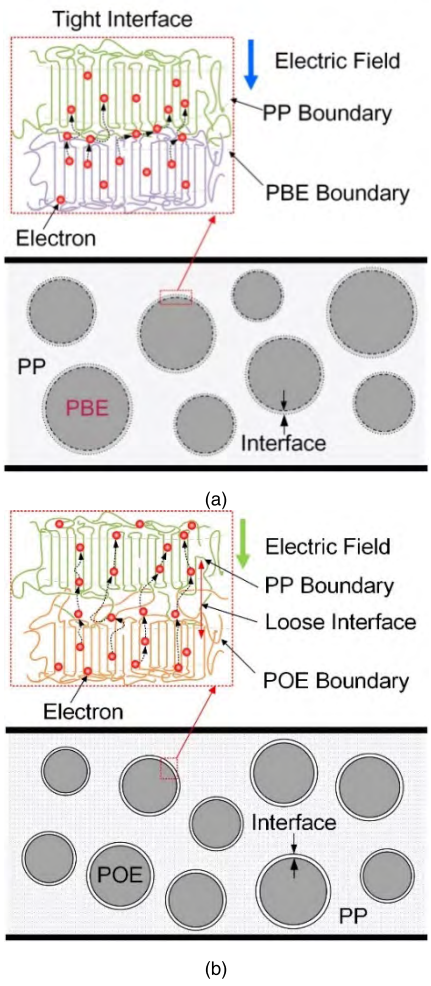

FIGURE 20. Schematic diagram of microscopic morphology at the interface between the PP and the elastomers. (a) PP/PBE blend. (b) PP/POE blend.

compatibility with PP matrix, the interfaces exhibit different features that remarkably affect the trap characteristics. As for the PP/PBE blend, since both PP and PBE molecular chains contain propylene groups, the Van der Waals' forces between them are strong. Thus the interaction of the molecular chains at the interface between PP and PBE is tight. Accordingly, as carriers are transported across the interface, they are likely to be captured by the traps formed due to molecular chains, as depicted in Fig.20(a), taking electrons as example. Since the disorder of molecular chains usually acts as chemical defect with deep trap center, the interface at PP/PBE exhibits deep trap. As a comparison, the trap characteristics at PP/POE interface should be different because of the bad compatibility. As can be seen in Fig.20(b), the molecular chains of PP and POE have weak interactions, the interface between them is therefore considered to be a loose one. This is confirmed by the SEM photo shown in Fig.17(c) and the double-peak feature with PO30 in Fig. 19 as well. Accordingly, as carriers are transported across the interface, the loosely bonded interface would allow the migration of charges easily. Such a loose interface should be recognized as physical defect that leads to the formation of shallow trap. Consequently, the PP/POE possesses shallower trap for both electron and hole than PP/PBE. It is therefore proposed that the deeper trap in PP/PBE blend should be attributed to the better compatibility between PP and PBE.

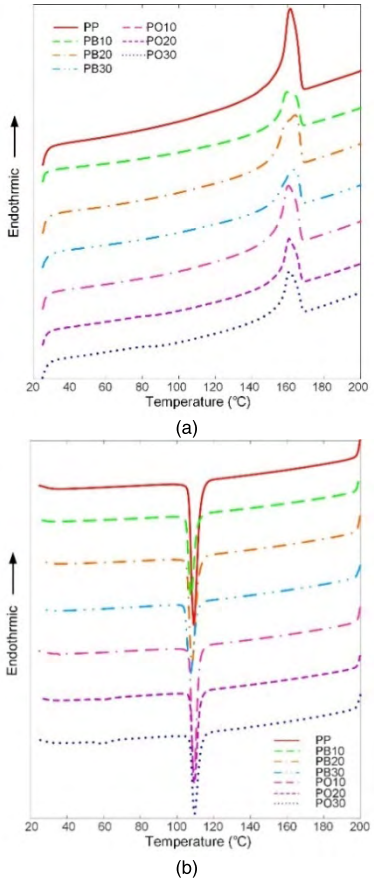

FIGURE 21. Melting and crystallization curves for PP and its blend samples. (a) Melting curves (b) Crystallization curves.

F. DSC ANALYSIS

In addition, it should be brought into mind that as the elastomer is blended into the virgin PP, the crystallization behavior may be varied such that the trap features of PP are altered. Fig.21 depicts the melting and the crystallization curves for virgin PP and PP/elastomer blends. It can be seen from Fig.21(a) that the melting behavior of PP is not remarkably influenced either by PBE or POE, the position of endothermic peak slightly varied with the elastomer content. Similar behaviors are observed with the crystallization process as well, as shown in Fig.21(b), no remarkable changes in the exothermic peaks among samples could be found. It reveals that the thermal property of PP is not significantly varied with the blending of PBE and POE. The T_m, the T_c and the $X_c\%$ are summarized in TABLE 4. The T_m is $\sim$161$\pm$2 °C (as a comparison, the T_m of XLPE is 133 °C [11]) whilst the T_c is $\sim$108$\pm$1 °C, which shows limited dependence upon the elastomer content. However, the Xc% appears to

TABLE 4. Summary of DSC data of the PP/elastomer blends.

Type	T_m(℃)	T_c (℃)	X_c(%)
PP	161.2	109.1	42.08
PB10	159.3	108.6	37.51
PB20	163.8	108.1	33.77
PB30	163.5	107.3	29.05
PO10	160.2	109.1	37.90
PO20	160.5	109.5	32.57
PO30	160.7	109.6	27.04

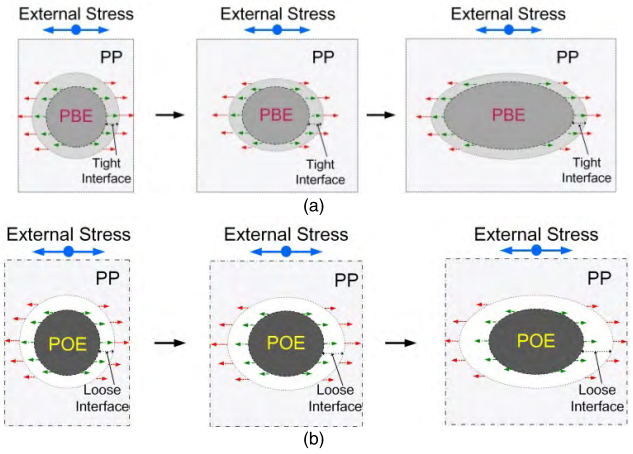

FIGURE 22. Deformation at the interface between the PP and the elastomers with the presence of external stress samples. (a) PP/PBE blend. (b) PP/POE blend.

decrease with the content grows from 0 wt% to 30 wt%, which should be ascribed to the fact that the crystallization process is restricted by the elastomer [14], [19]. As a result, free volume within the material would increase thus shallow traps are thought to be formed in the amorphous region [50]. It has been demonstrated that in semi-crystalline polymers, deep traps are mainly formed on the boundaries of spherulites and amorphous region, while the shallow traps are located in the amorphous region [50]. As the crystallinity decreases, the amorphous region increases, and the number of physical defects caused by structural defects in the amorphous region increases, leading to the shallower traps.

The compatibility between the PP matrix and the elastomer also has remarkable influence on the DC breakdown strength of the blends. For the PP/PBE blend, the DC breakdown strength is higher than PP/POE blend. The possible reason is that deeper traps are presented in PP/PBE blend and carriers are more difficult to be released from the trap to contribute to the impact ionization [51]. On the other hand, with regard to PP/POE blend, carriers are easily to de-trap and the breakdown is likely to occur more easily. The differences in the trap depths of the two blends are originated from both trap depth of virgin elastomer and compatibility with PP matrix, which in turn leads to the variation in DC breakdown strength of the blends.

The difference in flexibility between PP/PBE and PP/POE blends could be understood from the viewpoint of the compatibility mentioned above. The mechanism for flexibility improvement of polymer with elastomer has been extensively reported. A number of assumptions have been proposed to interpret the role of elastomer in modifying the flexibility of polymer, in which the crazing-shear zone, crazing branching and interfacial cavitation assumptions are included [52], [53]. The assumption of crazing-shear zone is usually employed to interpret the behavior of flexibility modification of PP with elastomer. In the PP/elastomer blend, the elastomer is dispersed as ''sea-island'' within the PP matrix, as depicted in Fig.17. When the blend is under external stress, the dispersed elastomer acts as stress center and induces a number of crazes and shear zones [53]. The crazes would absorb much impact energy, the elastomer and the formed shear band could cut off the further development of crazes as well, by which the flexibility of PP could be improved. In this work, due to the better compatibility between the PP matrix and the PBE, the stress could be transferred smoothly between the PP and the PBE through the tightly interacted interface, as is illustrated in the schematic diagram in Fig.22(a). As for the PP/POE blend, the loosely interacted interface may give rise to unmatched transfer of stress between the PP matrix and the POE, as shown in Fig.22(b), the enhancement in flexibility of PP is thus limited. As a result, the blend of PBE exhibits better performance in flexibility improvement of PP than that of POE.

In summary, it is suggested that the better compatibility between the PP matrix and the PBE should be responsible for its better electrical and mechanical properties as compared with the PP/POE blend. Owing to tight interaction at the interface, deeper trap depth could be found in the PP/PBE than the PP/POE which in turn results in its higher DC breakdown strength. Such a tight interaction also facilitates stress transfer between the PP matrix and the PBE elastomer, by which the flexibility of PP could be improved remarkably.

IV. CONCLUSIONS

Trap distribution and DC breakdown strength of PP/PBE blend have been investigated and compared with those of PP/POE blend. Elongation at break and tensile strength have also been estimated for the two types of blends. The main conclusions are summarized as follows,

1. With the increase of the elastomer content from 0 wt% to 30 wt% for both the PBE and the POE, the trap depth for both electron and hole tends to be shallower. The density at deep trap center basically decreases whereas the density at shallow trap center increases, which reveals that shallow trap would play a more important role in determining the electrical property of the blends. As a comparison, the trap depth of PP/PBE is deeper than that of PP/POE. The charge

transportation exhibits certain behavior that possibly follows the Poole-Frenkel mechanism.

2. With the growth of the elastomer content from 0 wt% to 30 wt%, the DC breakdown strength of both the PP/PBE and the PP/POE appears to decrease. Such a decrease is more remarkable for PP/POE than for PP/PBE. The addition of PBE with 10 wt% leads to a DC breakdown strength of ∼348 kV/mm, which is higher than that of XLPE.

3. With the increase of the elastomer content from 0 wt% to 30 wt%, the elongation at break for both blends increases significantly, while the tensile strength decreases. The elongation at break and the tensile strength for PP/PBE are higher than those for PP/POE, indicating that the improvement by PBE on toughness is better than by POE. In particular, the PB10 which contains only 10 wt% of PBE elastomer exhibits the elongation at break of ∼988.5% and the tensile strength of ∼38 N/mm^2, which is much better than those of XLPE.

4. In the blends, POE elastomer is dispersed as ''separated spots'', where abrupt boundary could be found at the PP/POE interface. The single peak feature in *tanδ* curve gradually becomes the double peak one as the POE content grows from 10 wt% to 30 wt%. With regard to PBE elastomer, it has better compatibility with PP that the boundary at the PP/PBE interface is indistinct, the single peak feature in *tanδ* curve appears for each PP/PBE sample with various elastomer contents. The PP/PBE exhibits stronger interaction at the interface than the PP/POE due to the better compatibility.

5. With the blending of the elastomers, the melting and the crystallization temperatures exhibit limited variation such that the thermal property of PP is not seriously affected by the toughening agents. However, as the elastomer content grows from 0 wt% to 30 wt%, the crystallinity tends to decrease, which would contribute to the shallowing of traps in the blends.

In this paper, we report on a type of elastomer, i.e. PBE, which has better compatibility with PP base material than POE. The addition of PBE with low content (typically 10 wt%) into PP is capable of forming the blend with remarkably improved flexibility and excellent electrical strength as compared with XLPE. The PBE may be promising as to modify the PP matrix for DC cable insulation. Furthermore, on the basis of test results obtained in this work, it could be expected that elastomer with good compatibility with PP matrix possibly results in significant improvement in mechanical property with appropriate electrical property for DC cable insulation. More research work is worth carrying out in this respect in the future.

ACKNOWLEDGMENT

The authors are grateful for the kind help on mechanical property measurement by Miss Zhengzheng Meng from Tianjin Electric Power Research Institute, Tianjin, China. They also appreciate the helpful suggestion from Prof. Xingyi Huang from Shanghai Jiao Tong University, China on the understanding of mechanical property of PP/elastomer blend. The author Yu Gao would like to thank Mr. Xinyu Wang who trained him to operate the Perkin Elmer DSC7 in the Tony Davies High Voltage Laboratory in the University of Southampton, the author Jing Li would like to appreciate the kind help in DMA analysis from Dr. Xiaohui Li in Tianjin University.

REFERENCES

[1] X. Y. Huang, Y. Fan, J. Zhang, and P. Jiang, ''Polypropylene based thermoplastic polymers for potential recyclable HVDC cable insulation applications,'' *IEEE Trans. Dielectr. Electr. Insul.*, vol. 24, no. 3, pp. 1446–1456, Jun. 2017.

[2] J.-W. Zha, Y.-H. Wu, S.-J. Wang, D.-H. Wu, H.-D. Yan, and Z.-M. Dang, ''Improvement of space charge suppression of polypropylene for potential application in HVDC cables,'' *IEEE Trans. Dielectr. Electr. Insul.*, vol. 23, no. 4, pp. 2337–2343, Aug. 2016.

[3] C. D. Green *et al.*, ''Thermoplastic cable insulation comprising a blend of isotactic polypropylene and a propylene-ethylene copolymer,'' *IEEE Trans. Dielectr. Electr. Insul.*, vol. 22, no. 2, pp. 639–648, Apr. 2015.

[4] B. W. Tuinema, J. L. Rueda, L. van der Sluis, and M. A. M. M. van der Meijden, ''Reliability of transmission links consisting of overhead lines and underground cables,'' *IEEE Trans. Power Del.*, vol. 31, no. 3, pp. 1251–1260, Jun. 2016.

[5] G.-Y. Kwon *et al.*, ''Offline fault localization technique on HVDC submarine cable via time–frequency domain reflectometry,'' *IEEE Trans. Power Del.*, vol. 32, no. 3, pp. 1626–1635, Jun. 2017.

[6] F. Yang, G. Sheng, Y. Xu, H. Hou, Y. Qian, and X. Jiang, ''Partial discharge pattern recognition of XLPE cables at DC voltage based on the compressed sensing theory,'' *IEEE Trans. Dielectr. Electr. Insul.*, vol. 24, no. 5, pp. 2977–2985, Oct. 2017.

[7] H. Liu, Y. Liu, Y. Li, P. Zheng, and H. Rui, ''Growth and partial discharge characteristics of electrical tree in XLPE under AC-DC composite voltage,'' *IEEE Trans. Dielectr. Electr. Insul.*, vol. 24, no. 4, pp. 2282–2290, Aug. 2017.

[8] X. Liu *et al.*, ''DC electrical breakdown dependence on the radial position of specimens within HVDC XLPE cable insulation,'' *IEEE Trans. Dielectr. Electr. Insul.*, vol. 24, no. 3, pp. 1476–1484, Jun. 2017.

[9] Y. Wang, G. Li, J. Wu, and Y. Yin, ''Effect of temperature on space charge detrapping and periodic grounded DC tree in cross-linked polyethylene,'' *IEEE Trans. Dielectr. Electr. Insul*, vol. 23, no. 6, pp. 3704–3711, Dec. 2016.

[10] T. Andritsch, A. Vaughan, and G. C. Stevens, ''Novel insulation materials for high voltage cable systems,'' *IEEE Electr. Insul. Mag.*, vol. 33, no. 4, pp. 27–33, Jul./Aug. 2017.

[11] C. D. Green, A. S. Vaughan, G. C. Stevens, S. J. Sutton, T. Geussens, and M. J. Fairhurst, ''Recyclable power cable comprising a blend of slow-crystallized polyethylenes,'' *IEEE Trans. Dielectr. Electr. Insul.*, vol. 20, no. 1, pp. 1–9, Feb. 2013.

[12] Y. Zhou, J. Hu, B. Dang, and J. He, ''Effect of different nanoparticles on tuning electrical properties of polypropylene nanocomposites,'' *IEEE Trans. Dielectr. Electr. Insul.*, vol. 24, no. 3, pp. 1380–1389, Jun. 2017.

[13] J. Diao, X. Huang, Q. Jia, F. Liu, and P. Jiang, ''Thermoplastic isotactic polypropylene/ethylene-octene polyolefin copolymer nanocomposite for recyclable HVDC cable insulation,'' *IEEE Trans. Dielectr. Electr. Insul.*, vol. 24, no. 3, pp. 1416–1429, Jun. 2017.

[14] B. Dang, J. He, J. Hu, and Y. Zhou, ''Large improvement in trap level and space charge distribution of polypropylene by enhancing the crystalline—Amorphous interface effect in blends,'' *Polym. Int.*, vol. 65, no. 4, pp. 371–379, Apr. 2016.

[15] K. Yoshino *et al.*, ''Novel properties of new type conducting and insulating polymers and their composites,'' *IEEE Trans. Dielectr. Electr. Insul.*, vol. 3, no. 3, pp. 331–344, Jun. 1996.

[16] I. L. Hosier, A. S. Vaughan, and S. G. Swingler, ''An investigation of the potential of polypropylene and its blends for use in recyclable high voltage cable insulation systems,'' *J. Mater. Sci.*, vol. 46, no. 11, pp. 4058–4070, Jun. 2011.

[17] A. R. Caramitu *et al.*, ''Study regarding mechanical, thermal and structural properties of some elastomeric polyamide blends destined to cable insulating,'' in *Proc. Int. Symp. Fundamentals Elect. Eng. (ISFEE)*, Bucharest, Romania, Nov. 2015, pp. 1–6.

[18] J.-W. Zha, Y. Wang, W.-K. Li, S.-J. Wang, and Z.-M. Dang, "Electrical properties of polypropylene/styrene-ethylene-butylene-styrene block copolymer/MgO nanocomposites," *IEEE Trans. Dielectr. Electr. Insul.*, vol. 24, no. 3, pp. 1457–1464, Jun. 2017.
[19] Y. Zhou, J. He, J. Hu, X. Huang, and P. Jiang, "Evaluation of polypropylene/polyolefin elastomer blends for potential recyclable HVDC cable insulation applications," *IEEE Trans. Dielectr. Electr. Insul*, vol. 22, no. 2, pp. 673–681, Apr. 2015.
[20] Y. Gao, J. Li, Y. Li, Y. Q. Yuan, S. H. Huang, and B. X. Du, "Effect of elastomer type on electrical and mechanical properties of polypropylene/elastomer blends," in *Proc. Int. Symp. Elect. Insul. Mater. (ISEIM)*, Toyohashi, Japan, vol. 2, Sep. 2017, pp. 574–577.
[21] Y. Gao, S. Huang, L. Y. Chen, H. Xu, and B. X. Du, "Effect of elastomer content on interface discharge behavior between polypropylene and silicone rubber under AC voltage," *High Voltage Eng.*, vol. 44, no. 9, pp. 2874–2880, Sep. 2018.
[22] *Vistamaxx 6202 Propylene-Based Elastomer*, Exxon Mobil Corp., Irving, TX, USA, 2010.
[23] A. T. Hoang, Y. V. Serdyuk, and S. M. Gubanski, "Mechanisms of surface potential decay on enamel wire coatings," *IEEE Trans. Dielectr. Electr. Insul.*, vol. 22, no. 6, pp. 3470–3480, Dec. 2015.
[24] S. Alam, Y. V. Serdyuk, and S. M. Gubanski, "Potential decay on silicone rubber surfaces affected by bulk and surface conductivities," *IEEE Trans. Dielectr. Electr. Insul.*, vol. 22, no. 2, pp. 970–978, Apr. 2015.
[25] P. Molinie, "A review of mechanisms and models accounting for surface potential decay," *IEEE Trans. Plasma Sci.*, vol. 40, no. 2, pp. 167–176, Feb. 2012.
[26] J. G. Simmons and M. C. Tam, "Theory of isothermal currents and the direct determination of trap parameters in semiconductors and insulators containing arbitrary trap distributions," *Phys. Rev. B, Condens. Matter*, vol. 7, no. 8, pp. 3706–3713, 1972.
[27] D. M. Min and S. T. Li, "Simulation on the influence of bipolar charge injection and trapping on surface potential decay of polyethylene," *IEEE Trans. Dielectr. Electr. Insul.*, vol. 21, no. 4, pp. 1627–1636, Aug. 2014.
[28] G. Teyssedre and C. Laurent, "Charge transport modeling in insulating polymers: From molecular to macroscopic scale," *IEEE Trans. Dielectr. Electr. Insul.*, vol. 12, no. 5, pp. 857–875, Oct. 2005.
[29] P. K. Watson, "The transport and trapping of electrons in polymers," *IEEE Trans. Dielectr. Electr. Insul.*, vol. 2, no. 5, pp. 915–924, Oct. 1995.
[30] H. Sjösted, S. M. Gubanski, and Y. V. Serdyuk, "Charging characteristics of EPDM and silicone rubbers deduced from surface potential measurements," *IEEE Trans. Dielectr. Electr. Insul.*, vol. 16, no. 3, pp. 696–703, Jun. 2009.
[31] J. Y. Li, F. S. Zhou, D. M. Min, S. T. Li, and R. Xia, "The energy distribution of trapped charges in polymers based on isothermal surface potential decay model," *IEEE Trans. Dielectr. Electr. Insul.*, vol. 22, no. 3, pp. 1723–1732, Jun. 2015.
[32] S. Kumara, B. Ma, Y. V. Serdyuk, and S. M. Gubanski, "Surface charge decay on HTV silicone rubber: Effect of material treatment by corona discharges," *IEEE Trans. Dielectr. Electr. Insul.*, vol. 19, no. 6, pp. 2189–2195, Dec. 2012.
[33] B. X. Du and Z. L. Li, "Surface charge and DC flashover characteristics of direct-fluorinated SiR/SiO_2 nanocomposites," *IEEE Trans. Dielectr. Electr. Insul.*, vol. 21, no. 6, pp. 2602–2610, Dec. 2014.
[34] *Standard Test Method for Tensile Properties of Thin Plastic Sheeting*, Standard ASTM D882-2010, ASTM Committee, 2010.
[35] D. Min, M. Cho, S. Li, and A. R. Khan, "Charge transport properties of insulators revealed by surface potential decay experiment and bipolar charge transport model with genetic algorithm," *IEEE Trans. Dielectr. Electr. Insul.*, vol. 19, no. 6, pp. 2206–2215, Dec. 2012.
[36] J. R. S. S. Kumara, Y. V. Serdyuk, and S. M. Gubanski, "Surface potential decay on LDPE and LDPE/Al2O3 nano-composites: Measurements and modeling," *IEEE Trans. Dielectr. Electr. Insul.*, vol. 23, no. 6, pp. 3466–3475, Dec. 2016.
[37] T.-C. Zhou, G. Chen, R.-J. Liao, and Z. Xu, "Charge trapping and detrapping in polymeric materials: Trapping parameters," *J. Appl. Phys.*, vol. 110, p. 043724, Aug. 2011.
[38] W.-W. Shen, H.-B. Mu, G.-J. Zhang, J.-B. Deng, and D.-M. Tu, "Identification of electron and hole trap based on isothermal surface potential decay model," *J. Appl. Phys.*, vol. 113, p. 083706, Feb. 2013.
[39] S. Li *et al.*, "Short-term breakdown and long-term failure in nanodielectrics: A review," *IEEE Trans. Dielectr. Electr. Insul.*, vol. 17, no. 5, pp. 1523–1535, Oct. 2010.
[40] S. Li, D. Min, W. Wang, and G. Chen, "Linking traps to dielectric breakdown through charge dynamics for polymer nanocomposites," *IEEE Trans. Dielectr. Electr. Insul.*, vol. 23, no. 5, pp. 2777–2785, Oct. 2016.
[41] B. X. Du, H. Xu, J. Li, and Z. Li, "Space charge behaviors of PP/POE/ZnO nanocomposites for HVDC cables," *IEEE Trans. Dielectr. Electr. Insul.*, vol. 23, no. 5, pp. 3165–3174, Oct. 2016.
[42] L. Boukezzi and A. Boubakeur, "Prediction of mechanical properties of XLPE cable insulation under thermal aging: Neural network approach," *IEEE Trans. Dielectr. Electr. Insul.*, vol. 20, no. 6, pp. 2125–2134, Dec. 2013.
[43] D. He, X. Wang, H. Liu, Q. Li, and G. Teyssèdre, "Space charge behavior in XLPE cable insulation under ac stress and its relation to thermo-electrical aging," *IEEE Trans. Dielectr. Electr. Insul.*, vol. 25, no. 2, pp. 541–550, Apr. 2018.
[44] Z. Kai *et al.*, "The mechanical properties of recyclable cable insulation materials based on thermo-plastic polyolefin blends," in *Proc. Int. Conf. Properties Appl. Dielectric Mater. (ICPADM)*, Sydney, NSW, Australia, Jul. 2015, pp. 532–535.
[45] M.-S. Xia, Z.-T. Yao, L.-Q. Ge, T. Chen, and H.-Y. Li, "A potential biofiller: The substitution effect of furfural modified clam shell for carbonate calcium in polypropylene," *J. Compos. Mater.*, vol. 49, no. 7, pp. 807–816, Mar. 2015.
[46] A. Hassan, N. A. Rahman, and R. Yahya, "Extrusion and injection-molding of glass fiber/MAPP/polypropylene: Effect of coupling agent on DSC, DMA, and mechanical properties," *J. Reinforced Plastics Compos.*, vol. 30, no. 14, pp. 1223–1232, Sep. 2011.
[47] E. A. Zubova, N. K. Balabaev, and L. I. Manevitch, "Molecular mechanisms of the chain diffusion between crystalline and amorphous fractions in polyethylene," *Polymer.*, vol. 48, no. 6, pp. 1802–1813, Mar. 2007.
[48] W. Wang, T. Takada, Y. Tanaka, and S. Li, "Trap-controlled charge decay and quantum chemical analysis of charge transfer and trapping in XLPE," *IEEE Trans. Dielectr. Electr. Insul.*, vol. 24, no. 5, pp. 3144–3153, Oct. 2017.
[49] K. Wu and C. Cheng, "Interface charges between insulating materials," *IEEE Trans. Dielectr. Electr. Insul.*, vol. 24, no. 4, pp. 2633–2642, Sep. 2017.
[50] X. Li, Q. Du, J. Kang, and D. Tu, "Influence of microstructure on space charges of polypropylene," *J. Polym. Sci. B, Polym. Phys.*, vol. 40, no. 4, pp. 365–374, Feb. 2002.
[51] Y. Nie, L. Yang, N. Zhao, D. Min, and S. Li, "Effect of surface state on DC breakdown of LDPE films," *IEEE Trans. Dielectr. Electr. Insul.*, vol. 24, no. 4, pp. 2522–2530, Sep. 2017.
[52] L. Zhang, C. Li, and R. Huang, "Toughness mechanism in polypropylene composites: Polypropylene toughened with elastomer and calcium carbonate," *J. Polym. Sci. B, Polym. Phys.*, vol. 42, no. 9, pp. 1656–1662, May 2004.
[53] A. van der Wal and R. J. Gaymans, "Polypropylene–rubber blends: 5. Deformation mechanism during fracture," *Polymer*, vol. 40, no. 22, pp. 6067–6075, Oct. 1999.

YU GAO (M'10) was born in Xinmin, Liaoning, China, in 1981. He received the Ph.D. degree from the School of Electrical and Information Engineering, Tianjin University, Tianjin, China, in 2009. Since 2012, he has been an Associate Professor in the field of high voltage and electrical insulation technology. Since 2017, he has been an Academic Visitor with the University of Southampton, U.K. His current research interests include ageing phenomena of polymer insulating materials, pulsed power technology and its application in environment engineering, and over voltage mechanism and protection.

JING LI was born in Zhangjiakou, Hebei, China, in 1994. She received the B.Sc. degree from Tianjin University, Tianjin, China, in 2017, where she is currently pursuing the M.S. degree in electrical engineering. Her research interests focus on the application of thermal plastic material polypropylene as high-voltage direct current cable insulation and space charge measurement by means of surface potential decay and pulsed electro-acoustic methods.

YANQIU YUAN was born in Weifang, Shandong, China, in 1994. He received the B.Sc. degree from the Shandong University of Technology, Shandong, China, in 2016. He is currently pursuing the M.S. degree in electrical engineering with Tianjin University. He is engaged in research on surface charge measurement in solid dielectrics and ageing mechanisms of polymer material for recyclable cable insulation.

SHIHAO HUANG was born in Dandong, Liaoning, China, in 1993. He received the M.S. degree from Tianjin University, Tianjin, China, in 2018. His research interests focus on trap characterization in solid dielectrics and ageing of polymer film insulation.

BOXUE DU (M'00–SM'04) received the M.E. degree in electrical engineering from Ibaraki University in 1993 and the Ph.D. degree from the Tokyo University of Agriculture and Technology in 1996. He was an Associated Professor with the Niigata College of Technology, Japan. He is currently a Professor with the Department of Electrical Engineering, School of Electrical and Information Engineering, Tianjin University, China. His main research interests are dielectric failure mechanisms of polymer insulating materials, electrical insulation technology, and partial discharge measurements. He is a member of IEEJ and a Senior Member of CSEE.